International Journal of Engineering Trends and Technology
ISSN: 2231–5381 / https://doi.org/10.14445/22315381/IJETT-V72I3P130

Volume 72 Issue 3, 349-357, March 2024

Original Article

Experimental and Numerical Investigations on the Novel Twisting Metamaterial Architected with Diamond-Shaped Lattices

Abderrahim Barhoumi[1*], Mohamed Atify[2], Ganzosch Gregor[3], Abdelhai Rahmani[1]

[1]*Advanced Materials and Applications Laboratory (LEM2A), Moulay Ismail University, Meknes, Morocco*.
[2]*Department of Innovation and Smart Technologies (IST), Polydisciplinary Faculty, Sultan Moulay Slimane University of Beni Mellal, Morocco.*
[3]*Institute of Mechanics, Faculty 5, Berlin University of Technology, Berlin, Germany*.

[*]*Corresponding Author : a.barhoumi@edu.umi.ac.ma*

Received: 18 November 2023 Revised: 20 February 2024 Accepted: 29 February 2024 Published: 17 March 2024

Abstract *- Twisting metamaterials have structures that convert axial tensile or compressive loads into rotational motion. The present paper proposes an improved compression-torsion metamaterial whose unit cell comprises two diamond-shaped lattices linked by four chirally inclined rods. Numerical and experimental studies are performed to examine the effect of geometric and intrinsic metamaterial parameters on twist behavior in compression deformation. The results showed that the improved metamaterial exhibits excellent compression-torsion conversion, positioning it as an ideal option for practical industrial uses, such as biomechanics, aerospace engineering, microelectronics, and sensor and actuator technologies.*

Keywords *- Mechanical metamaterial, Compression-torsion coupling, Additive manufacturing, Finite elements analysis, Diamond-shaped lattice.*

1. Introduction

Nowadays, metamaterials have gained the attention of many experimental, theoretical, and computational research groups. Their development has made great strides thanks to the advent of new additive manufacturing techniques [1]. Architectural materials, known as metamaterials, have special characteristics beyond the base materials. The emergence of this field of research has benefited various engineering applications, such as intelligent actuators [2], pantographic structures [3], biomedical implants [4], bandgaps [5], [6], and battery electrodes [7]. Among them, Mechanical metamaterials[8] have been widely studied as a new branch of metamaterials due to their abnormal mechanical properties, including negative values of the Poisson's ratio [9], excellent indentation resistance[10], negative compressibility[11], negative stiffness [12], [13], and compression-torsion coupling effects. The latter converts an axial load (compression or stretching) into twist deformation. It is worth noting that this degree of freedom is exclusive to two-dimensional (2D) [14] and three-dimensional (3D) [15] chiral mechanical metamaterials and cannot be described by the classical Cauchy theory. The micropolar continuum theory [16] is often used to describe the rotational mechanical behaviors induced by the chirality of the internal microstructures.

Frenzel et al. [17] made the first steps in this field by designing a chiral twist metamaterial microstructured with cubic unit cells and proved by different approaches that the torsion angle per unit of axial deformation exceeded 2◦/%. Kadic et al. [18] have shown that the Willis static equations qualitatively describe the chiral effects of homogeneous materials with cubic symmetry by introducing a single additional parameter with respect to the linear Cauchy elasticity.

In this context, Xu et al. [19] suggested a modular design method by subdividing the unit cell into many independent design units for 3D chiral metamaterials with tunable compression-torsion behaviors. Numerical and theoretical studies were conducted by Lemkalli et al. [20] on a modified 3D chiral cubic structure with perforated edges to characterize the static and dynamic responses of the torsional behavior of this metamaterial. More recently, Montazeri et al. [21]designed a cubic metamaterial with a twisting effect along the three primary axes.

Several research studies have been conducted to improve the twisting performance, and various metamaterial structures have been developed.

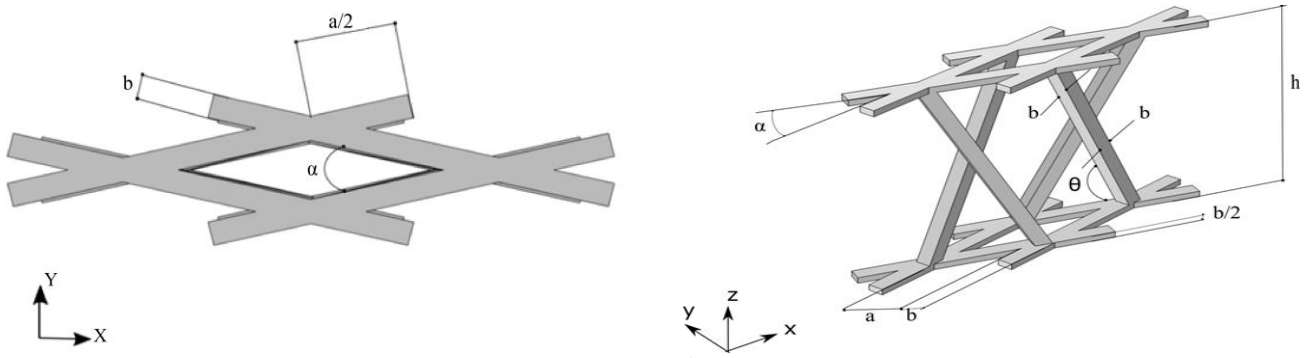

Fig. 1 Isometric and top views of the optimized unit cell.

Compared with other metamaterial structures, 3D chiral metamaterials assembled by replicating a unit cell of Z-shaped geometry and having bending-dominated ligaments during deformation are the most widely used. They are commonly referred to as 3D Z-structures [22], [23], [24], [25], [26] and have great potential for property tunability and good compression-torsion performance. By exploiting the distinctive properties of this type of structure, Zhong et al. [27] proposed a new design. They found that the key factors influencing compression-twisting in a multicellular metamaterial structure are determined by the unit cells' twisting angle, the total number of transverse cells, and the number of layers according to the height. The unit cell of this structure has been the subject of a numerical geometric optimization of previous study has led to significant improvements in the twist estimated at 111%. Such a result represents a step towards solving the problem of loss of scalability, which is a major challenge for twisting metamaterials and deserves to be studied. In this paper, the finite element model has been experimentally validated, and a novel three-dimensional mechanical metamaterial whose unit cell consists of two diamond-shaped lattices connected by four chirally inclined rods has been proposed. A complementary numerical study was carried out to investigate the influence of other parameters on the overall compression-torsion behavior. The results showed that the improved metamaterial exhibits excellent compression-torsion conversion, making it a good candidate for practical applications in industry, such as biomechanical and aerospace engineering, microelectronics, sensors, and actuators.

2. Structure Model

The numerical study of geometric optimization conducted previously led to a unit cell represented in Figure 1. These are two rhombic-shaped lattices linked by four chirally oriented struts inclined at an angle θ to induce torsion in the metamaterial under the effect of compression or tension. The distance between the middle plane of the adjacent two layers is h. The cross sections of the eight struts and four inclined rods are square with side length b. θ = arctan (h/a) represents the angle between the tilted rods and the x-axis. Each rhombus has a side length a and a characteristic angle α.

3. Test Setup and Material Properties

3.1. Fabrication of Samples

To perform the compression-torsion test, four CAD models of unit cells were designed with α angles of 30°, 45°, 60° and 70°. During the uniaxial compression of the specimen, the torsion can be influenced by the contact of the loading platforms and both the upper and lower faces. Therefore, as shown in Figure 2, a mirror symmetry layer in the middle is introduced to avoid this problem and to give them the possibility of free and simultaneous rotation.

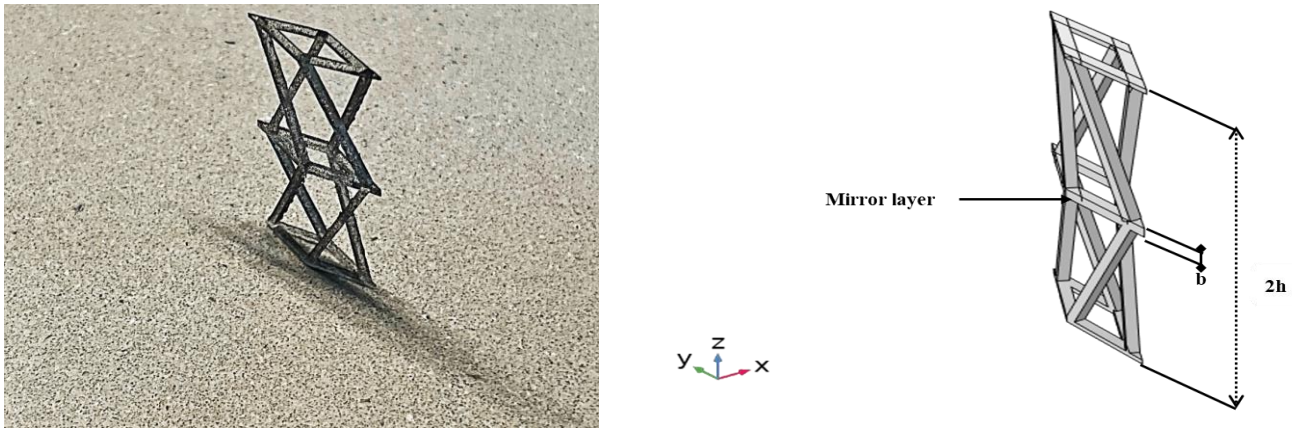

(a) **(b)**

Fig. 2 Printed model (a) and CAD model (b)

Figures 3 and 4 show specimens fabricated by additive manufacturing using stereo-lithographic appearance (SLA) technology. The 3D printer Form 2 from the American manufacturer Formlabs (see Figure 4) is used in this work.

All the samples are printed keeping the same printing parameters; the efficiency of the resin curing depends essentially on it. Indeed, for high-quality printing, the thickness of the printing layer is fixed at 100µm. In accordance with ISO527-1(2012)[29], two standard dog bone-shaped specimens were printed to obtain the mechanical properties of the base material (UV-cured EPOXY resin).

3.2. Properties of the Parent Material

First, to ascertain the basic material's mechanical characteristics (EPOXY resin), uniaxial tensile tests are carried out on a "Zwick Roell" tensile/compression machine with a load capacity of 2.5 kN, as shown in Figure 5. Compression and tensile tests are performed using the two-dimensional digital image correlation (2D-DIC) technique with precise strain measurements using GOM Correlate software.

The dog-bone-shaped samples are pixilated by paint spraying, as seen in Figure 6, and a digital camera (Canon EOS M6 Mark II) is used to capture and save the images during the test. It can capture up to 14 images per second. The specimens are loaded at a constant rate of 0.5 mm/min until failure. Referring to the above standard, the average values of the modulus of elasticity and the Poisson's ratio calculated are 2.58GPa and 0.39, respectively. In addition, although the material selected for the study is EPOXY resin, the mechanical properties of the constituent material have a negligible effect on the compression-torsion, so other materials with a large elastic regime can be used, [30],[28],[18].

3.3. Quasi-Static Compressive Tests of Unit Cell Samples as Printed

The pre-painted models are tested on the same universal tension/compression machine to validate the finite element simulation results. The applied longitudinal compression displacements were controlled during the test, and the compression speed was kept at 3 mm/min, corresponding to the quasi-static process.

Fig. 3 The experimental specimens as manufactured

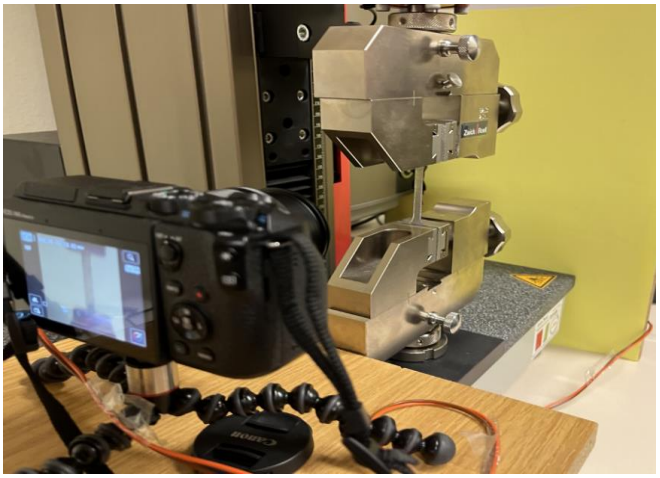

Fig. 5 Components of the experimental setup

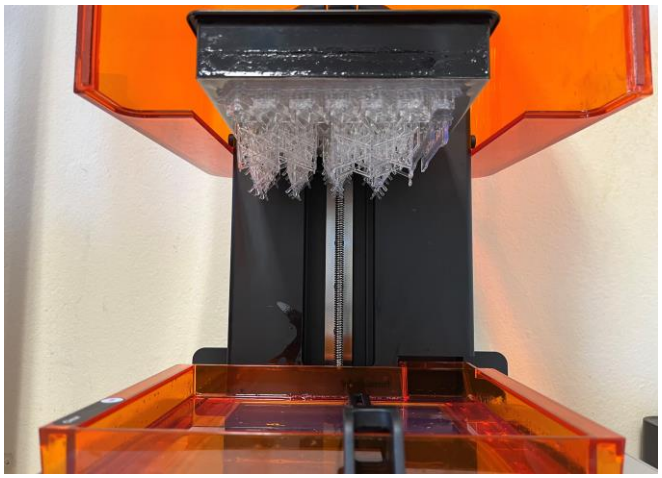

Fig. 4 Form 2 (3D) printer and experimental specimens as manufactured

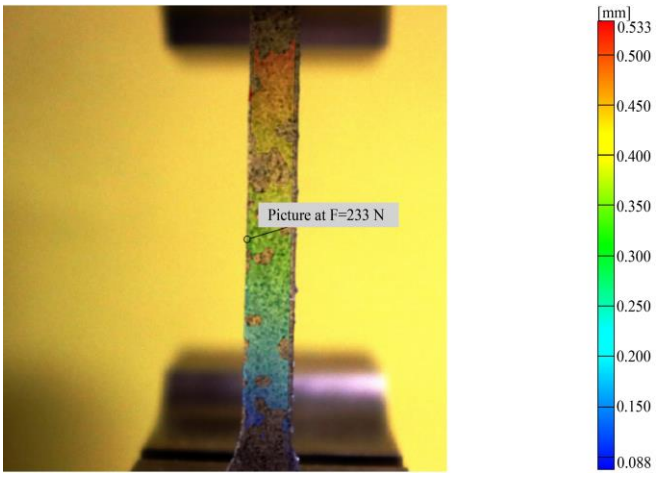

Fig. 6 Uniaxial tensile tests on dog bone specimens

The camera was aimed at the mirror layer to take a picture of every 0.1 mm of longitudinal deformations, and 107 pictures were captured. The measurement setup and boundary conditions are shown in Figure 7. The sketch in Figure 8 illustrates that, as the sample is twisted, point P moves towards point M. The distance between the center of the sample (point O) and point P was L, which can be calculated as a function of the side a and the angle α by relation (1). Obviously, in this application, the 2D-DIC technique could not directly evaluate the displacement Δx. Thus, the following expression (2) for the torsion angle β of the midplane depends only on the intrinsic parameters of the cell and the displacement Δy.

$$L = a \cdot \cos\left(\frac{\alpha}{2}\right) \quad (1)$$

$$\beta = \left(\frac{180}{\Pi}\right) \cdot \arcsin\left(\frac{\Delta y}{a \cdot \cos\left(\frac{\alpha}{2}\right)}\right) \quad (2)$$

Where Δx and Δy are the distances between the point P and point M along the x and y axes, respectively. Furthermore, a is the side length of the rhombus, and α is its characteristic angle.

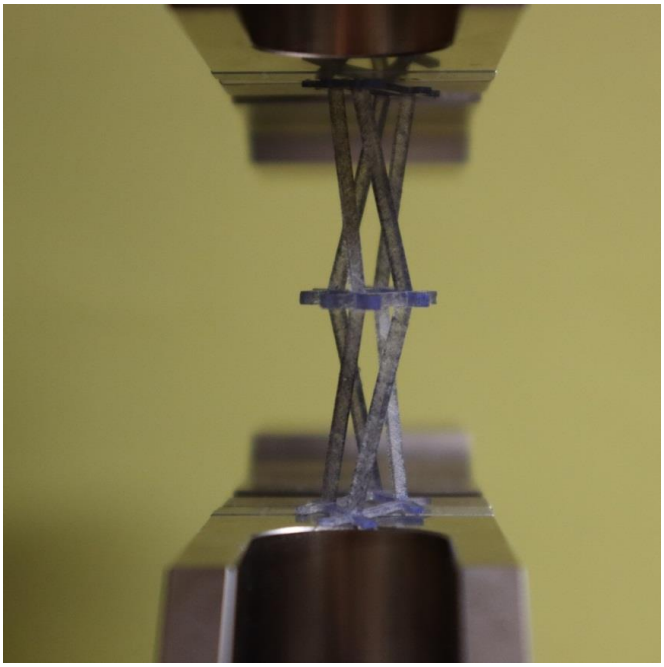

Fig. 7 Specimen under axial compressive load

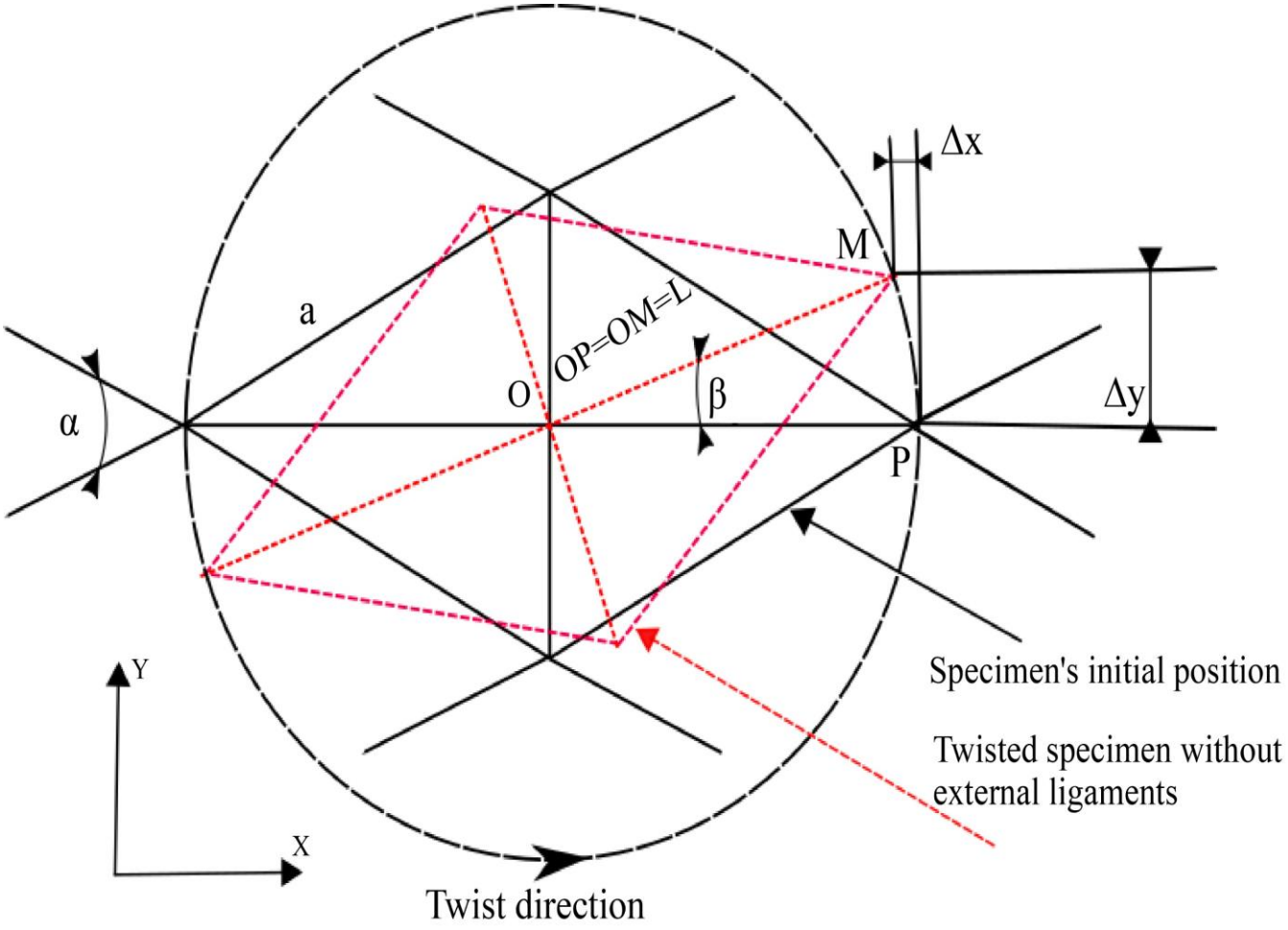

Fig. 8 Top view sketch of the twisted unit cell

It should be noted that the twist angle per unit axial compressive strain φ is calculated by the ratio of the torsion angle β to the axial strain ε_z along the z-axis (3)

$$\varphi = \left(\frac{\beta}{\varepsilon_z} \right) \quad (3)$$

4. Numerical Simulation Characteristics

All numerical simulation work was performed using the COMSOL Multiphysics software. The material and geometric parameters of the finite element models are the same as those of the experiments. Thus, the properties of the base material are defined as Young's modulus E=2.6 GPa and Poisson's ratio 0.4. The deformations are small enough for all models that our study is conducted exclusively in the reversible elastic domain.

A uniaxial load is applied to the upper face in the longitudinal direction of the models, imposing the desired displacement, and the bottom boundary is fixed. The other deformations, apart from the one along z, will constitute the output results, which will be used later in calculations of torsion angles. A mesh sensitivity study was carried out to guarantee that the computational results are mesh-independent.

5. Results and Discussion

5.1. Model Validation

As expected, the results showed that the greater the deformation, the greater the twist angle, but the linearity of this variation is verified around a deformation of 1%. The graph in Figure 9 compares the two approaches—the smaller the characteristic angle α of the rhombus, the greater the torsion angle. Admittedly, the number of unit cells manufactured is only four. However, since consecutive angles of a rhombus are supplementary, each sample of a specific angle α corresponds to another angle (π-α). Thus the total number of specimens will be eight: 30°, 45°, 60°,70°,150°,135°,120° and 110°.

Overall, the numerical results and the experimental findings (EXP) coincide well, indicating that the finite element model may be validated. However, printed metamaterial structures can exhibit unavoidable manufacturing defects. Consequently, some minor differences appear between the FEM and EXP results.

The validity of the finite element model used is verified. In the following, an additional parametric study is performed. The purpose of this section is to study the impact of the metamaterial unit cell's relative characteristics on its torsion numerically (FEM) and to investigate the dependence of the torsion angle when these parameters change independently of each other, with a relative uniaxial compressive strain not exceeding 1%.

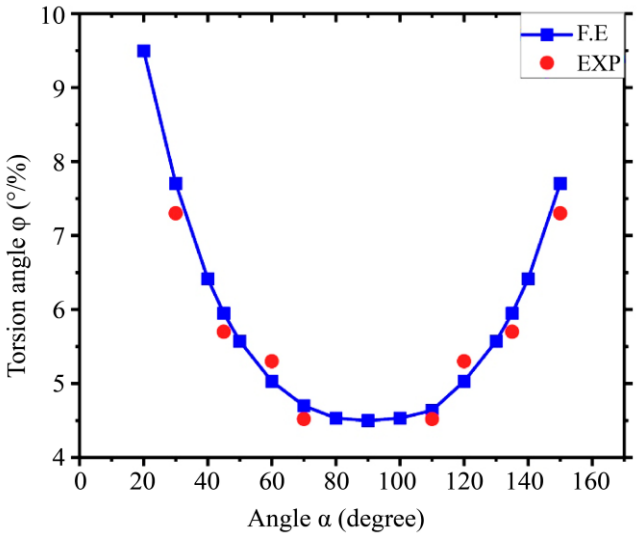

Fig. 9 Comparison of finite element simulations and experimental results of torsion angle variation with angle α at εz =1%

5.2. Effect of height "h"

The angle of inclination of the rods "θ" is related to the height "h" by the relation (4):

$$\theta = \operatorname{atan}\left(\frac{h}{a}\right) \quad (4)$$

The optimization of the rod tilt angle "θ" in reference [27] led to the choice h=2a, with a corresponding optimal angle θ=63.43 degrees.

As shown in Figure 10, simultaneous variation of "h" and "a" has almost no effect on the torsion angle.

Table 1. Geometric parameters of unit cell structure

h (mm)	a (mm)	b (mm)	θ (°)
24	12	1.5	63.43
25	12.5	1.5	63.43
26	13	1.5	63.43
27	13.5	1.5	63.43
28	14	1.5	63.43
29	14.5	1.5	63.43
30	15	1.5	63.43
31	15.5	1.5	63.43
32	16	1.5	63.43
33	16.5	1.5	63.43
34	17	1.5	63.43
35	17.5	1.5	63.43
36	18	1.5	63.43

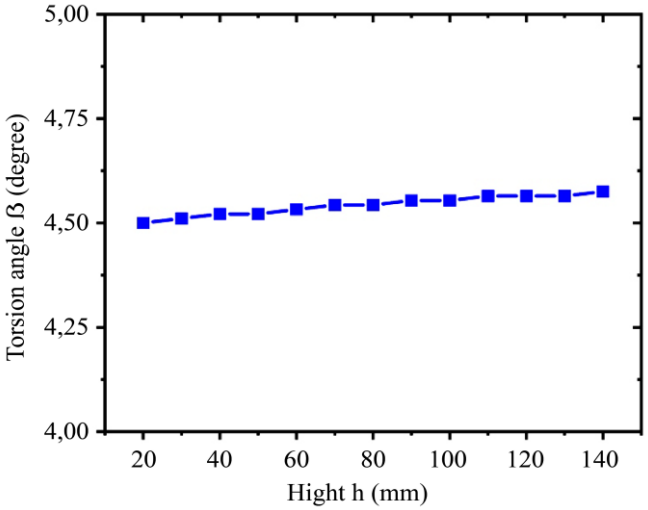

Fig. 10 Effect of height h on the torsion angle β, εz =1%.

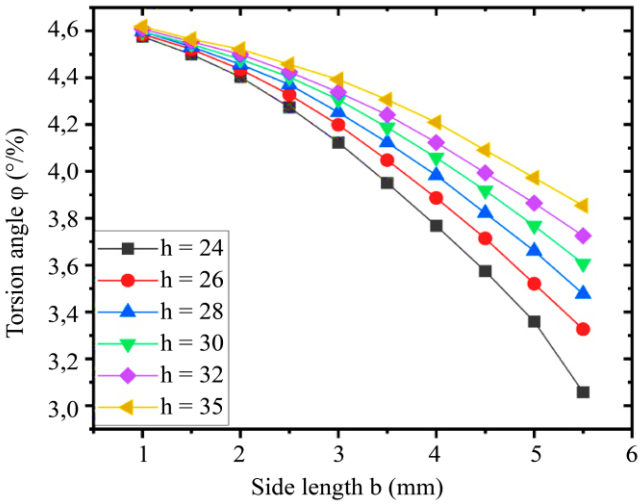

Fig. 11 Effect of the size of the inclined rod cross-section on the torsion angle β, ε_z =1%.

5.3. Effect of the Size of the inclined Rod Cross-Section

The influence of side length b on the twist angle is illustrated in Figure 11 and is studied for different values of height h ranging from 24 to 35 mm, giving rise to 60 finite element models. Table 2 shows an example of geometrical parameters when h is 30 mm. If the square cross-section varies from 1mm2 to 30.25 mm2, the twist angle decreases by about 34% when the torsion varies from 4.58°/% to 3.06°/% (for h=24mm), and the decrease is more significant as the height "h" is minimal.

5.4. Effect of the cross-sectional shape of inclined rods

Two geometric shapes are studied, as shown in Figure 12: the square section with side "b" and the circular section with diameter "b".

Figure 13 shows the dimension b's effect on the twist angle for two different cross-sections (square and circular). By fixing the height "h" at 24 mm and varying "b" from 1 to 5.5 mm, the torsion angle decreases, almost identically, with increasing side "b". In fact, the geometric shape of the cross-sections has no significant effect on twists between 1 and 5mm.

Table 2. Geometric parameters of unit cell structure for h=30mm

h (mm)	a(mm)	b (mm)	Cross-section (mm^2)	θ (°)
30	15	1	1	63.43
30	15	1.5	2.25	63.43
30	15	2	4	63.43
30	15	2.5	6.25	63.43
30	15	3	9	63.43
30	15	3.5	12.25	63.43
30	15	4	16	63.43
30	15	4.5	20.25	63.43
30	15	5	25	63.43
30	15	5.5	30.25	63.43

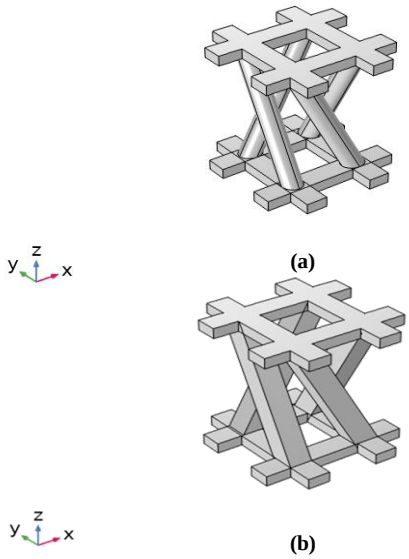

Fig. 12 Geometry of the unit cell for inclined rods with circular (a) and square (b) cross sections

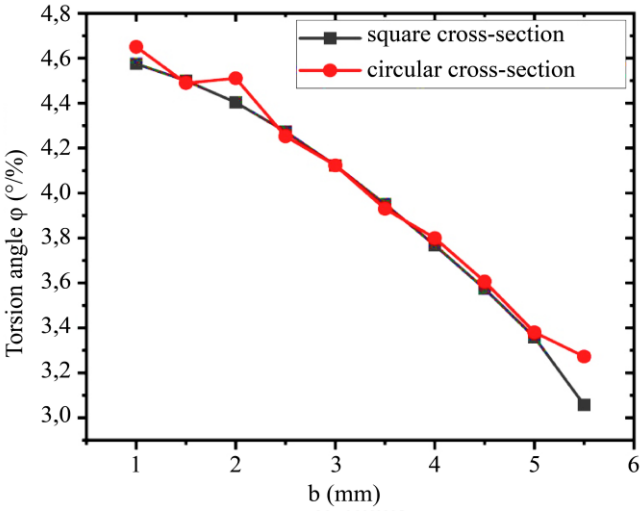

Fig. 13 Variation of twist angle with dimension b for height h=24mm

5.5. Performance of the Improved Compression-Torsion Metamaterial

The novel metamaterial structure will be based on the optimized unit cell. According to the results found in the previous sections, the characteristic angle α of the rhombus is the most influential factor on the twist angle, and a comparative increase estimated at 111% was achieved. To prevent inclined rods from overlapping when deforming, an angle α=30 degrees is used, as shown in Figure 14(a). A first layer in the xy-plane will be obtained by connecting the cells together directly and without ligaments at the edges. Thus, Figure 14(b) illustrates the compression-torsion metamaterial constructed by adding layers along the z direction.

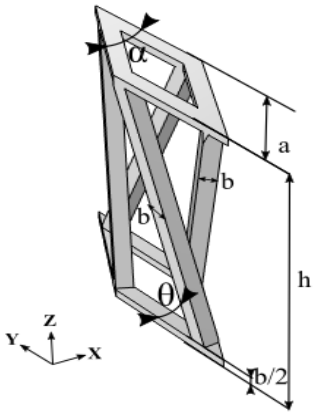

(a)

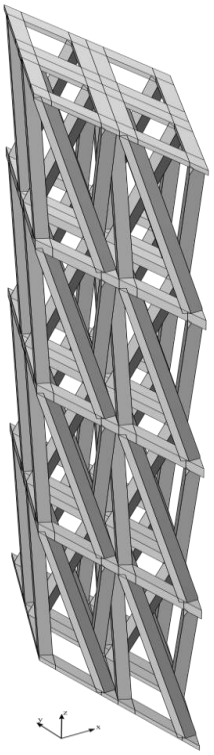

Fig. 14 Geometry of the improved 3D metamaterial, (a) unit cell, (b) multi-cell (4 unit cells x 4 vertical layers)

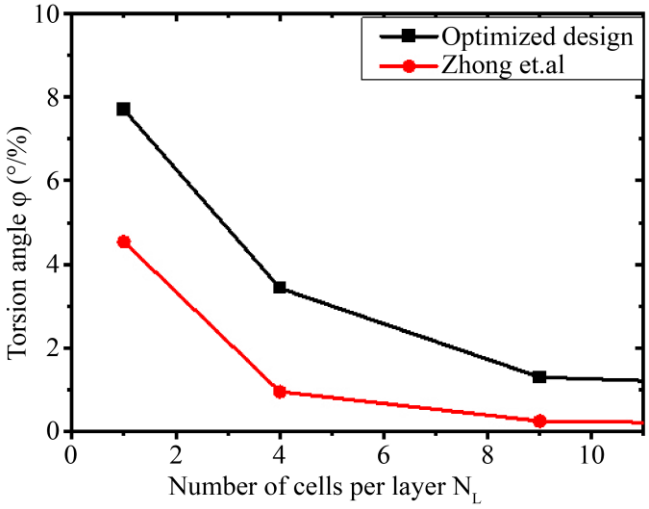

Fig. 15 Variation of twist angle with number of cells per layer N_L at ε_z =1%.

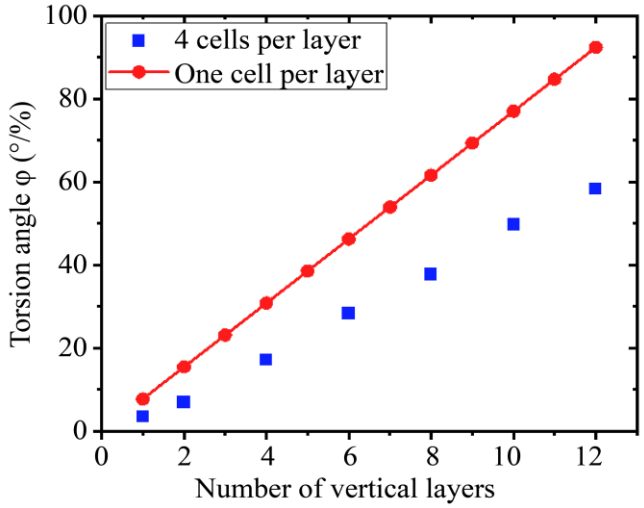

Fig. 16 Variation of twist angle with number of vertical layers at ε_z =1%.

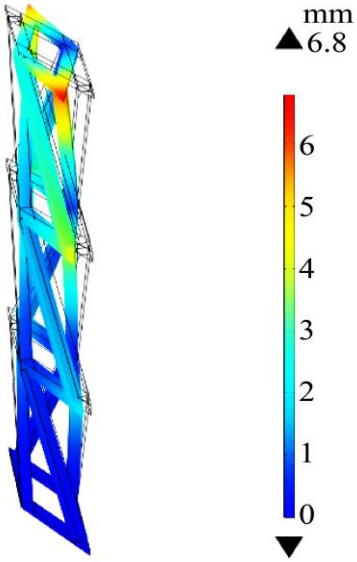

Fig. 17 Deformation image along the z direction at ε_z =1%.

The overall torsion of the 3D mechanical metamaterial depends on how the unit cells are connected horizontally and vertically. To study the influence of the number of cells per layer, noted in the following NL, a numerical study has been carried out under the same conditions as above, in which the effect of vertical stacking of layers is excluded by working on a single layer in the xy-plane. All models underwent the same -1% deformation. Figure 15 shows a comparison between the present design and its initial counterpart [27]. Indeed, the transverse constraint increases with the multiplication of cells per layer. However, when the unit cell has very good compression-torsion behavior, as in this case with 7.7 degrees per unit of axial strain, the tendency for the assembled structure to decrease is not very strong. To conclude this study, the results of the numerical calculations presented in Figure 16 highlight the influence of the vertical superposition of the layers. The variation of the twist as a function of the number of vertical layers is clearly linear in the case of a single cell. This behavior can be explained by the absence of transverse constraints caused by the existence of neighboring cells, as can be seen in Figure 17.

When the number of cells in the transverse plane equals 4, adding vertical layers amplifies the twist by progressively compensating for these transverse constraints.

6. Conclusion

This paper proposes an improved compression-torsion metamaterial whose unit cell consists of two diamond-shaped lattices connected by four chirally tilted rods. The study focused on the influence of intrinsic geometrical parameters of the unit cell, and the finite element model was experimentally validated—the smaller the characteristic angle α of the rhombus, the greater the torsion angle.

However, the overlapping of the inclined rods during deformation forced us to settle on an optimum angle of 30 degrees. The influence of the cross-sectional size of these rods on twist behavior is also developed by FEM, indicating that the twist angle increases with decreasing cross-sectional size, whether circular or square. In addition, the comparison between the improved metamaterial and its initial counterpart showed a significant reduction in transverse constraint.

References

[1] Zhiyuan Huang, Guangbin Shao, and Longqiu Li, "Micro/Nano Functional Devices Fabricated by Additive Manufacturing," *Progress in Materials Science*, vol. 131, 2023, [CrossRef] [Google Scholar] [Publisher Link]

[2] Ying Jiang et al., "Auxetic Mechanical Metamaterials to Enhance Sensitivity of Stretchable Strain Sensors," *Advanced Materials*, vol. 30, no. 12, 2018. [CrossRef] [Google Scholar] [Publisher Link]

[3] Francesco dell'Isola et al., "Pantographic Metamaterials: An Example of Mathematically Driven Design and of its Technological Challenges," *Continuum Mechanics and Thermodynamics*, vol. 31, no. 4, pp. 851-884, 2019. [CrossRef] [Google Scholar] [Publisher Link]

[4] S.S. Nene et al., "Biocorrosion and Biodegradation Behavior of Ultralight Mg-4Li-1Ca (LC41) Alloy in Simulated Body Fluid for Degradable Implant Applications," *Journal of Materials Science*, vol. 50, pp. 3041-3050, 2015. [CrossRef] [Google Scholar] [Publisher Link]

[5] Luca D'Alessandro et al., "A Design strategy to Match the Band Gap of Periodic and Aperiodic Metamaterials," *Scientific Reports*, vol. 10, no. 1, pp. 1-13, 2020. [CrossRef] [Google Scholar] [Publisher Link]

[6] Zhiwen Ren et al., "SMP-Based Multi-Stable Mechanical Metamaterials: From Bandgap Tuning to Wave Logic Gates," *Extreme Mechanics Letters*, vol. 42, 2021. [CrossRef] [Google Scholar] [Publisher Link]

[7] James R. Wheeler, Jack N. Brill, and Lee E. Miller, "Lattice for a Battery Electrode Substrate," *US4477546A*, pp. 1-6, 1984. [Google Scholar] [Publisher Link]

[8] Johan Christensen et al., "Vibrant Times for Mechanical Metamaterials," *MRS Communications*, vol. 5, no. 3, pp. 453-462, 2015. [CrossRef] [Google Scholar] [Publisher Link]

[9] Minghui Fu, Fengming Liu, and Lingling Hu, "A Novel Category of 3D Chiral Material with Negative Poisson's Ratio," *Composites Science and Technology*, vol. 160, pp. 111-118, 2018. [CrossRef] [Google Scholar] [Publisher Link]

[10] L.L. Hu, M.Z. Zhou, and H. Deng, "Dynamic Indentation of Auxetic and Non-Auxetic Honeycombs under Large Deformation," *Composite Structures*, vol. 207, pp. 323-330, 2019. [CrossRef] [Google Scholar] [Publisher Link]

[11] Ray H. Baughman et al., "Materials with Negative Compressibilities in One or More Dimensions," *Science*, vol. 279, no. 5356, pp. 1522-1524, 1998. [CrossRef] [Google Scholar] [Publisher Link]

[12] Xiaojun Tan et al., "Novel Multi-Stable Mechanical Metamaterials for Trapping Energy through Shear Deformation," *International Journal of Mechanical Sciences*, vol. 164, 2019. [CrossRef] [Google Scholar] [Publisher Link]

[13] Tan Xiaojun et al., "Reusable Metamaterial Via Inelastic Instability for Energy Absorption," *International Journal of Mechanical Sciences*, vol. 155, pp. 509-517, 2019. [CrossRef] [Google Scholar] [Publisher Link]

[14] X.N. Liu, G.L. Huang, and G.K. Hu, "Chiral Effect in Plane Isotropic Micropolar Elasticity and its Application to Chiral Lattices," *Journal of the Mechanics and Physics of Solids*, vol. 60, no. 11, pp. 1907-1921, 2012. [CrossRef] [Google Scholar] [Publisher Link]

[15] Chan Soo Ha, Michael E. Plesha, and Roderic S. Lakes, "Chiral Three-Dimensional Isotropic Lattices with Negative Poisson's Ratio:

Chiral 3D Isotropic Lattices with Negative Poisson's Ratio," *Solid State Physics B*, vol. 253, no. 7, pp. 1243-1251, 2016. [CrossRef] [Google Scholar] [Publisher Link]

[16] A. Cemal Eringen, *Theory of Micropolar Elasticity*, Microcontinuum Field Theories, Springer, New York, pp. 101-248, 1999. [CrossRef] [Google Scholar] [Publisher Link]

[17] Tobias Frenzel, Muamer Kadic, and Martin Wegener, "Three-Dimensional Mechanical Metamaterials with a Twist," *Science*, vol. 358, no. 6366, pp. 1072-1074, 2017. [CrossRef] [Google Scholar] [Publisher Link]

[18] Muamer Kadic et al., "Static Chiral Willis Continuum Mechanics for Three-Dimensional Chiral Mechanical Metamaterials," *Physical Review B*, vol. 99, no. 21, 2019. [CrossRef] [Google Scholar] [Publisher Link]

[19] Weiyun Xu et al., "3D Chiral Metamaterial Modular Design with Highly-Tunable Tension-Twisting Properties," *MaterialsToday Communications*, vol. 30, 2022. [CrossRef] [Google Scholar] [Publisher Link]

[20] Brahim Lemkalli et al., "Mapping of Elastic Properties of Twisting Metamaterials onto Micropolar Continuum Using Static Calculations," *International Journal of Mechanical Sciences*, vol. 254, 2023. [CrossRef] [Google Scholar] [Publisher Link]

[21] Amin Montazeri, Fardad Homafar, and Maryam Mahnama, "A Novel 3D Compression-Torsion Mechanical Metamaterial with Cubic Cells based on Askew Star Mechanism: Design, Simulation, and Experimental Validations," *Mechanics of Advanced Materials and Structures*, pp. 1-10, 2022. [CrossRef] [Google Scholar] [Publisher Link]

[22] Rongchang Zhong, Binbin Zheng, and Minghui Fu, "A Novel Strategy for Constructing 3D Dislocated Chiral Metamaterial with Negative Poisson's Ratio," *Advanced Engineering Materials*, vol. 23, no. 3, 2021. [CrossRef] [Google Scholar] [Publisher Link]

[23] Chuanqi Yang et al., "Theoretical Analysis on the Stiffness of Compression-Torsion Coupling Metamaterials," *Extreme Mechanics Letters*, vol. 46, 2021. [CrossRef] [Google Scholar] [Publisher Link]

[24] Xiang Li, Zhenyu Yang, and Zixing Lu, "Design 3D Metamaterials with Compression-Induced-Twisting Characteristics Using Shear-Compression Coupling Effects," *Extreme Mechanics Letters*, vol. 29, 2019. [CrossRef] [Google Scholar] [Publisher Link]

[25] Bin-Bin Zheng et al., "A Novel Metamaterial with Tension-Torsion Coupling Effect," *Materials & Design*, vol. 171, pp. 1-9, 2019. [CrossRef] [Google Scholar] [Publisher Link]

[26] Gaojian Lin et al., "Buckling of Lattice Columns made from Three-Dimensional Chiral Mechanical Metamaterials," *International Journal of Mechanical Sciences*, vol. 194, 2021. [CrossRef] [Google Scholar] [Publisher Link]

[27] Rongchang Zhong et al., "A Novel Three-Dimensional Mechanical Metamaterial with Compression-Torsion Properties," *Composite Structures*, vol. 226, 2019. [CrossRef] [Google Scholar] [Publisher Link]

[28] Liang Wang, and Hai-Tao Liu, "3D Compression–Torsion Cubic Mechanical Metamaterial with Double Inclined Rods," *Extreme Mechanics Letters*, vol. 37, 2020. [CrossRef] [Google Scholar] [Publisher Link]

[29] International Organization for Standardization, *Plastics: Determination of Tensile Properties-General principles- Part 1*, ISO, pp. 1-23, 2012. [Google Scholar] [Publisher Link]

[30] Wei Zhang et al., "Mechanical Properties of the Three-Dimensional Compression-Twist Cellular Structure," *Journal of Reinforced Plastics and Composites*, vol. 39, no. 7-8, pp. 260-277, 2020. [CrossRef] [Google Scholar] [Publisher Link]